J. Fluid Mech. (1974), *vol.* 66, *part* 3, *pp.* 553–576
Printed in Great Britain

The vortex-street wakes of vibrating cylinders

By OWEN M. GRIFFIN
AND STEVEN E. RAMBERG
Naval Research Laboratory, Washington, D.C. 20375

(Received 31 August 1973 and in revised form 9 May 1974)

The strength (initial circulation) and spacing of vortices in the wake of a circular cylinder have been obtained for conditions under which the body undergoes lateral vibrations. The vibrations of the cylinder were at all times synchronized with those in the wake, thereby suppressing the natural Strouhal frequency in favour of a common synchronized or 'locked-in' frequency for the body–wake system. All experiments were performed at a Reynolds number of 144 or 190. An inverse relation between the initial circulation K and the length l_F of the vortex formation region was obtained for cylinder oscillations of up to 50 % of a diameter, at vibration frequencies both above and below the Strouhal shedding frequency. The initial circulation K of the vortices was increased by as much as 65 %, at $l_F = 1{\cdot}6$ diameters, from the stationary-cylinder value of K corresponding to $l_F = 3{\cdot}2d$. An increase in the rate Λ of vorticity generation of 80 % from the stationary-cylinder wake value was obtained with the cylinder vibrating at 30 % of a diameter and 110 % of the Strouhal frequency. Both flow-visualization and hot-wire results show that the lateral spacing of the vortex street decreases as the vibration amplitude of the cylinder is increased, but that the longitudinal vortex spacing is independent of changes in amplitude. The longitudinal spacing, however, varies inversely with the vibration frequency. The street approaches a single line of vortices of alternating sign as the amplitude of vibration approaches values near a full cylinder diameter, and secondary vortex formation at these large amplitudes is associated with the vanishing lateral spacing of the street. Observation of the wake has elucidated the mechanism of vortex formation; the entrainment processes in the formation region have been observed at small intervals over a cycle of the cylinder's motion.

1. Introduction

The periodic flow separation and vortex formation that accompany the flow past a bluff obstacle have been observed for many years, but still many questions relating to the mechanism of vortex formation remain unanswered. If one of the natural frequencies of the body immersed in the flow is near the vortex shedding frequency, then self-excited resonant vibrations can occur if the damping of the system is sufficiently low. There is also a range of frequencies near the Strouhal frequency of vortex shedding where forced vibrations of the body cause the vortex shedding and body frequencies to lock together, or synchronize. This means that the cylinder and wake have the same characteristic frequency and that the

Strouhal frequency, relating to the vortex shedding from a stationary cylinder, is suppressed. Synchronization (or wake capture, as it is sometimes called) takes place when the vibration amplitude reaches a critical threshold and is accompanied by large correlations in the phase of the vortex shedding along the cylinder span.

Vortex-excited vibrations are often the cause of costly construction delays and failures in offshore structures, and the 'strumming' motions of towed and moored underwater platforms will degrade the data-gathering performance of these systems. A recent Euromech Colloquium on bluff bodies and vortex shedding (1970) in Cambridge† and a symposium on flow-induced structural vibrations (1972) in Karlsruhe attest to the contemporary practical importance of these fluid–structural interaction phenomena.

The body–wake system behaves as a nonlinear self-excited oscillator with the wake as the oscillator and the cylinder forced to vibrate. This interaction between the body motion and the wake should be evidenced by changes in the vortex formation, strength and spacing that accompany different conditions of oscillation, with the real origin of vortex-excited oscillations lying in the mechanism of the vortex formation and shedding process. In the present paper we investigate the changes in the vortex formation, strength and spacing that accompany different conditions of cylinder vibration. These parameters are obtained by matching both mean and r.m.s. velocity profiles with a mathematical model for the vortex street. The effects of the cylinder vibrations are then further investigated by means of a detailed flow-visualization study of the vortex formation and spacing within the regime of synchronization.

2. Related investigations

Some investigations have been made of the interaction between a vibrating bluff body and its vortex wake, but since these vibrations are often the cause of costly problems, more extensive studies of vortex-excited and forced synchronized oscillations are of both practical and fundamental importance. Berger & Wille (1972) have recently summarized contemporary work relating to the generation of oscillatory wake flows, and other reviews of the present state of knowledge relating to vortex-excited and forced lateral oscillations can be found in papers by King, Prosser & Johns (1973), Parkinson (1972) and Toebes (1969).

Despite the insight that can be obtained from the use of some means of flow visualization, there have been very few visual studies of the interaction between a vibrating bluff body and its wake. The results of Wood & Kirmani (1970) and of Wood (1971) deal with the heaving vibrations of blunt-based aerofoils under conditions of forced lock-in. Honji & Taneda (1968*a*, *b*) have observed the changes in the wake that accompany the lateral vibrations of circular cylinders at large amplitudes of motion, again under conditions of lock-in. The original flow-visualization study of a cylinder vibrating laterally with the vortex and vibration frequencies synchronized was published by Koopmann (1967*a*) for

† See Mair & Maull (1971).

Reynolds numbers between 100 and 300, and more recently Griffin & Votaw (1972) have provided further flow-visualization results in this same Reynolds number regime. Koopmann (1967*b*) has photographed the wake of a freely vibrating cylinder and these results have been published as part of a more extensive study of the vortex-excited oscillations of circular cylinders (Griffin, Skop & Koopmann 1973).

Information on the strength of shed vortices is sparse for stationary bodies, and no studies of the effects of cylinder vibrations on vortex strength have previously been made. One of the most complete works for stationary bodies is that of Berger (1964), who measured the strength and spacing of vortices at several downstream displacements in the stable region behind a stationary cylinder at a Reynolds number $Re = 150$. Schaefer & Eskinazi (1959) had earlier studied the stationary-cylinder wake at Reynolds numbers below 125 and measured the vortex strength at one downstream position for $Re = 62$. More recently, Bloor & Gerrard (1966) obtained the strengths of turbulent vortices in the wakes of stationary cylinders at $Re = 2000$ and 16 000, and compared their results with the semi-empirical theory of Roshko (1954), who proposed a universal similarity parameter for characterizing the wakes of stationary bluff bodies of various shapes.

The introduction of transverse vibrations, either vortex-excited or forced, into the body–wake system increases the complexities involved in any attempt to determine such wake parameters as the vortex strength, spacing and core radius. All of the latter are dependent on the length of the formation region and the distance from the end of the formation region to the measurement point. The papers by Griffin (1971), Griffin & Votaw (1972) and Griffin (1973), hereafter denoted as I, II and III, have investigated the dependence of the formation length and wake structure on the amplitude and frequency of vibration. The experiments also showed that the formation length is an appropriate scaling length for the vortex wake of an oscillating body, and that the wake is composed of the three classical regimes of the Kármán street: the formation, stable and unstable regions. These regimes are found at Reynolds numbers up to 350 for the vibrating cylinder, whereas they have been observed at Reynolds numbers only up to 125 for the stationary cylinder.

3. Experimental methods and procedure

The experiments reported in this paper were performed in an open-jet wind tunnel with a 75×75 mm exit and a 20:1 contraction section. DISA hot-wire anemometers (model 55D01) and low interference hot-wire probes (model 55F01) were employed for the flow measurements. The hot-wire signal was carefully linearized in the speed range of interest with a DISA linearizer (model 55D10), so that quantitative velocity measurements could be interpreted with confidence. Smooth circular cylinders, 2·4, 3·2 and 4·0 mm in diameter, were used in the experiments and were mounted in a vibration-isolated shaker at the tunnel exit section. The details of the wind tunnel and its supporting equipment have been described in I and II.

The photographs were taken by introducing an aerosol of submicron-sized particles into the wind tunnel. The tracer is generated simply by bubbling compressed air through liquid di-2 (ethylhexyl phthalate), or DOP. A more complete discussion of the flow-visualization system, including measurements of light scattering in the aerosol and some further applications, has been given by Griffin, Ramberg, Votaw & Kelleher (1973). The flow field was illuminated by two strobes driven by the same sine-wave generator as was used to vibrate the cylinder. Since the vortex shedding and cylinder frequencies were synchronized, the light flashing was also locked into the wake. A variable-phase channel on the sine-wave generator allowed the vortex street to be photographed at any instant within a cycle of the cylinder motion, and the initial position of the cylinder (as seen during the flash) was also adjustable by means of a time delay on the strobe system.

4. Co-ordinate system and notation

The origin of the co-ordinates, except as noted in § 5, is at the equilibrium position of the cylinder centre, with displacements in the free-stream direction denoted by x and those perpendicular to the free-stream direction denoted by y. The cylinder's diameter is denoted by d and the amplitude of oscillation (peak to peak) by a. For the stationary cylinder the natural vortex shedding (Strouhal) frequency is denoted by f_s, and f corresponds to the oscillation frequency of the cylinder. Since all of the experiments correspond to the regime of frequency synchronization, or lock-in, the cylinder and vortex shedding frequencies are equal. The relation between the vibration and vortex frequencies during lock-in is illustrated in figure 1. When the frequency of forced oscillation becomes about 80 % of the Strouhal frequency, the body and wake have the same characteristic frequency. The two frequencies remain locked together as the frequency is increased to about 120 % of the Strouhal frequency. For frequencies above this limit the wake unlocks from the vibration of the body. The measured velocity fluctuations (r.m.s.) are denoted by u, the mean free-stream velocity by U and the local mean velocity by $U(y)$. The Reynolds number is $Re = Ud/\nu$, where ν is the kinematic viscosity of the fluid. Under natural shedding conditions the Strouhal number is $St = f_s d/U$ and a wake shedding parameter used to characterize the lock-in phenomenon is $St^* = St(1+a/d)f/f_s$.

5. Flow in the near wake of a vibrating cylinder

5.1. *The formation and stable regions of the wake*

It is generally agreed that a close relation exists between the flow in the near wake and the fluid forces on a vibrating cylinder, and several physical criteria have been identified for determining the initial position of a fully formed vortex in the base region of a bluff body. Among these criteria are the following.

(i) The minimum of the mean pressure on the wake centre-line $y = 0$ (Roshko 1954).

(ii) The maximum velocity fluctuation at the second harmonic of the shedding frequency, on the wake centre-line (Bloor & Gerrard 1966).

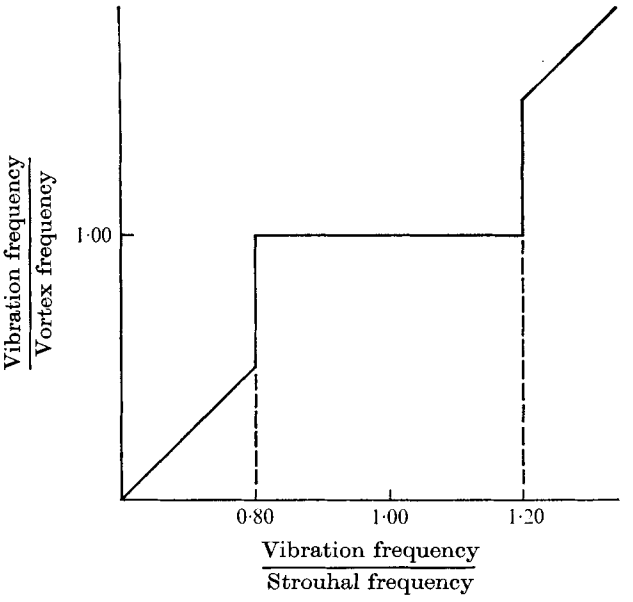

FIGURE 1. Schematic diagram of the lock-in relation for transverse forced oscillations of a bluff body in a uniform stream. The amplitude of the body motion is assumed to be fixed at some value within the synchronized regime.

(iii) The minimum lateral spacing, near the body base, of the region of maximum vortex velocity fluctuation (Schaefer & Eskinazi 1959; Bearman 1965).

These criteria yield essentially the same value for the formation length l_F and they can be measured with a pressure or hot-wire probe. The effects of lateral vibrations on vortex formation length have been discussed in I and II, and the results may be briefly summarized as follows. The formation length decreases systematically with increased amplitude of vibration, whereas the effects of frequency changes are twofold. When the vibration frequency is decreased to a value less than the Strouhal frequency, the length of the formation region is increased; conversely, when the vibration frequency becomes greater than the Strouhal frequency the scale of the formation region is reduced. The formation-region length is expressed as a function of both the vibration amplitude and frequency by

$$\frac{l_F}{d_F} = -3{\cdot}2 - 3{\cdot}3 \ln St^*, \quad St^* = St\frac{f}{f_s}\left(1+\frac{a}{d}\right), \tag{1}$$

cf. III, for Reynolds numbers up to at least 350 and for conditions of synchronization between the vortex shedding and vibration frequencies. The wake width d_F in (1) is defined by the lateral spacing between the maxima of velocity fluctuations at $x = l_F$.

A difficult problem arises during any attempt to compare systematically the properties of vortex-street wakes under different flow conditions, because the measurements are dependent on the relative distance from the point at which the

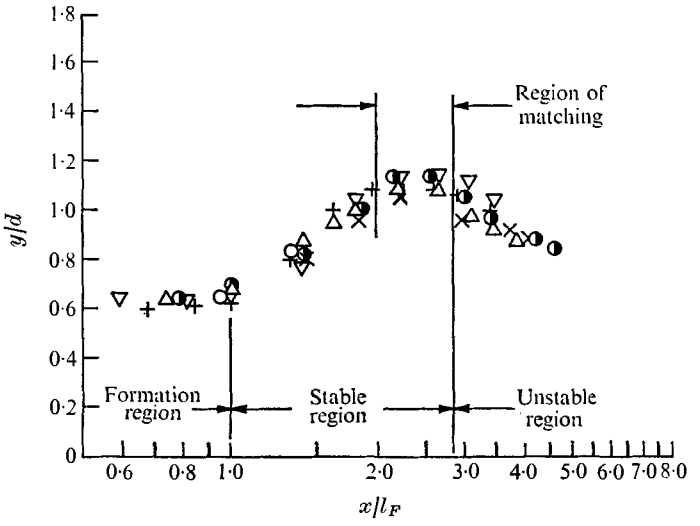

FIGURE 2. Distribution of the regions of maximum velocity fluctuation as a function of the scaled downstream distance x/l_F, at a Reynolds number of 144. The cylinder and vortex shedding frequencies are synchronized.

	○	+	△	◑	▽	×
*St**	0·178	0·199	0·231	0·263	0·208	0·254
f/*fs*	1·00	1·00	1·00	1·00	0·90	1·10
a/*d*	0	0·12	0·30	0·48	0·30	0·30

vortices are formed, i.e. on the formation length l_F. This problem is compounded when any alterations are made in the mechanism of the vortex shedding. Such changes may include mass addition and splitter plates in the base region of a bluff body, or flow-induced and forced synchronized oscillations. Such a problem arises in the present case because the formation-region length at $Re = 144$ is reduced from 3·1 to 1·6 diameters as the amplitude of vibration is increased from zero to half a diameter, and any interpretations based on wake measurements made at a single downstream value of x/d can be seriously misleading.

The vortex wake of a cylinder vibrating under conditions of synchronism can be scaled by the formation length, as plotted in figure 2 with results obtained at a Reynolds number of 144. Since the wake patterns for all values of the vibration amplitude and frequency fall on a single curve, the effects of the vibrations can be systematically assessed by making measurements at constant multiples of x/l_F. Each determination will then account for the changes in the position of vortex formation, and the difficulties mentioned above will be minimized.

5.2. *A mathematical model for the stable region*

The downstream portion of the stable region outlined in figure 2 offers suitable locations at which to measure the strength, age and spacing of the vortices, with due regard being given to the constraints imposed in the previous section. In order to account for the effects of viscosity, the potential vortices at an arbitrary number of positions in the street can be replaced by Hamel–Oseen vortices. The

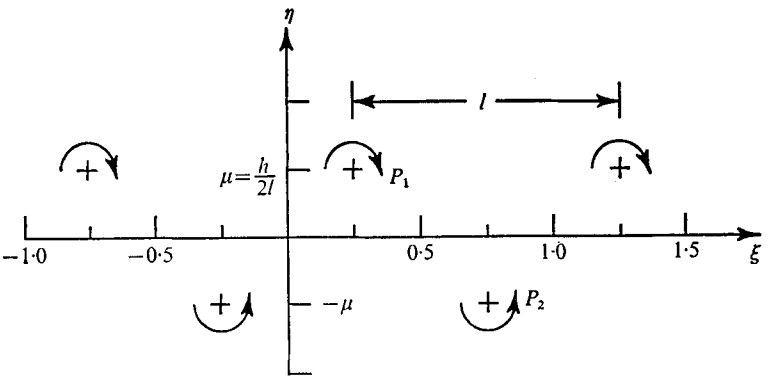

FIGURE 3. Co-ordinate system for an infinite vortex street with constant lateral spacing h and longitudinal spacing l. The vortices at P_1 and P_2 are replaced by Hamel–Oseen viscous vortices in the velocity components listed in table 1. The vortex-street velocity potential (uncorrected for viscosity) is

$$\psi = \frac{iK}{2\pi} \ln\left(\frac{\sin[\pi(z'-z_0')]}{\sin[\pi(z'+z_0')]}\right) + Ulz',$$

where $z' = \xi + i\eta$ and $z_0' = \frac{1}{4} + i\mu$.

circumferential velocity and vorticity fields of each viscous Hamel–Oseen vortex are, respectively,

$$u_\theta = \frac{K}{2\pi r}\{1 - \exp[-1{\cdot}26(r^2/r_*^2)]\}, \quad r_*^2 = 5{\cdot}04\nu t, \tag{2}$$

$$\zeta = \frac{1{\cdot}26K}{\pi r_*^2} \exp[-1{\cdot}26(r^2/r_*^2)], \tag{3}$$

where r_* represents the radial distance from the vortex centre to the maximum of u_θ, t the age of the vortex and K the initial circulation. The basic Kármán street corrected in this way for the effects of viscosity is an appropriate model for the stable region of the vibrating-cylinder wake since the flow is essentially two-dimensional.

The complex velocity potential for an inviscid street of vortices, taken at some initial time $t = 0$ and in co-ordinates fixed relative to the equilibrium position of the cylinder, is given in figure 3. At this initial time the vortices in the upper row are at the positions $(m+\frac{1}{4})+i\mu$ and the vortices in the lower row are at the positions $(m-\frac{1}{4})-i\mu$, for $m = 0, +1, +2,$ etc. The velocity components are given by

$$u_{\text{pot}} - iv_{\text{pot}} = d\Psi/dz, \quad z = lz'.$$

The final results in table 1 represent those obtained with only the potential vortices at the positions P_1 and P_2 replaced by viscous vortices, since the replacement of others was subsequently found to be unnecessary. Some recent computations by Chaplin (1972) have shown that two Hamel–Oseen vortices are sufficient for small values of the vortex core radius, $r_* \leqslant 0{\cdot}3l$, and the results discussed in § 6 are within this range. The velocity components u' and v' relative to co-ordinates ξ and η fixed with respect to the equilibrium position of the cylinder are listed in table 1 and the vortex-street configuration is outlined in figure 3.

$$\frac{u'}{U}(x', y') = 1 - \left(\frac{K}{Ul}\right) \frac{\cosh 2\pi\mu(\sinh 2\pi\mu - \sin 2\pi\xi \sinh 2\pi\eta)}{\sinh^2 2\pi\mu + \sinh^2 2\pi\eta + \cos^2 2\pi\xi - 2\sinh 2\pi\mu \sin 2\pi\xi \sinh 2\pi\eta}$$
$$- \left(\frac{K}{2\pi Ul}\right) \frac{\exp\{-\alpha[(\xi-\frac{1}{4})^2 + (\eta-\mu)^2]\}}{(\xi-\frac{1}{4})^2 + (\eta-\mu)^2}(\eta-\mu) + \left(\frac{K}{2\pi Ul}\right) \frac{\exp\{-\alpha[(\xi-\frac{3}{4})^2 + (\eta+\mu)^2]\}}{(\xi-\frac{3}{4})^2 + (\eta+\mu)^2}(\eta+\mu)$$

$$\frac{v'}{U}(x', y') = \left(\frac{K}{Ul}\right) \frac{\cosh 2\pi\mu \cos 2\pi\xi \cosh 2\pi\eta}{\sinh^2 2\pi\mu + \sinh^2 2\pi\eta + \cos^2 2\pi\xi - 2\sinh 2\pi\mu \sin 2\pi\xi \sinh 2\pi\eta}$$
$$+ \frac{K}{2\pi Ul} \frac{\exp\{-\alpha[(\xi-\frac{1}{4})^2 + (\eta-\mu)^2]\}}{(\xi-\frac{1}{4})^2 + (\eta-\mu)^2}(\xi-\tfrac{1}{4}) - \left(\frac{K}{2\pi Ul}\right) \frac{\exp\{-\alpha[(\xi-\frac{3}{4})^2 + (\eta+\mu)^2]\}}{(\xi-\frac{3}{4})^2 + (\eta+\mu)^2}(\xi-\tfrac{3}{4})$$

$$\left(\frac{q'}{U}\right)^2 = \left(\frac{u'}{U}\right)^2 + \left(\frac{v'}{U}\right)^2, \quad \lim_{\substack{\eta\to\mu \\ \xi\to\frac{1}{4}}} \left(\frac{q'}{U}\right) = \frac{fl}{U}$$

$$\mu = \frac{h}{2l}, \quad \alpha = \frac{l^2}{4\nu t}, \quad \xi = \frac{x'}{l}, \quad \eta = \frac{y'}{l}$$

TABLE 1. Velocity components in the stable region of the vortex-street wake. Co-ordinates corresponding to the velocity distribution are given in figure 3

Several assumptions are implied in the use of the vortex-street model presented above. The core radius r_* or age t is assumed to be constant as the street moves over one cycle; thus the results represent an average value of r^* or t at a given downstream displacement. Likewise, the transverse spacing h of the vortices is constant in the mathematical formulation. This assumption is valid so long as the model is matched with experiment in the downstream part of the stable region as outlined in figure 2. The finite length of the real vortex street for $x > 0$ is also disregarded in the formulation, but this approximation is also shown to be acceptable in the downstream portion of the stable region where the lateral motion of the vortices is small. Weihs (1972) has shown that a vortex-street model with constant lateral spacing has utility as an initial step towards further understanding of the interaction between a vibrating bluff body and its wake.

The velocity distribution in table 1 has been used to evaluate the vortex-street parameters at two downstream positions in the stable region for each of three values of the cylinder amplitude and frequency of vibration. There are four unknown parameters to be evaluated: the vortex strength $K/2\pi$ (m^2/s), core radius r_* (m), lateral spacing h (m) and longitudinal spacing l (m). The last, l, was measured directly. The three remaining parameters are determined here from the experimental profiles by matching the measured and computed mean and r.m.s. velocity profiles at nine equally spaced lateral displacements between 0 and 2·0d from the centre-line of the wake. The solution is chosen as the set of parameters K, r_* and h/l that results in a minimum of the error function

$$E = \sum_{j=1}^{9} \left(\frac{u_{m,j} - u_{c,j}}{u_{m,j}}\right)^2 + \left(\frac{U_{m,j} - U_{c,j}}{U_{m,j}}\right)^2. \tag{4}$$

A related criterion was employed by Bloor & Gerrard (1966) in a study of the turbulent vortex street. The computed velocities u_c and U_c are obtained by

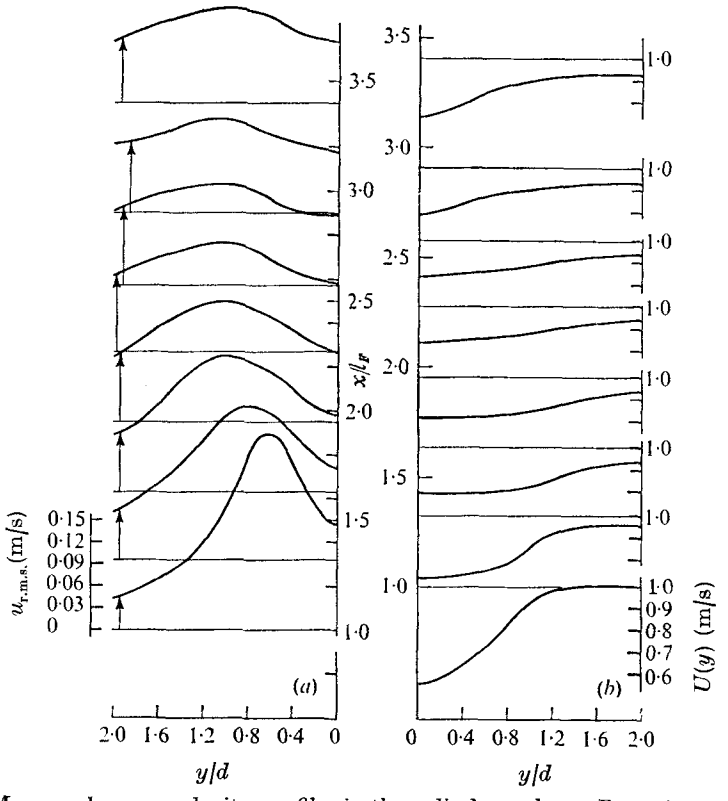

FIGURE 4. Mean and r.m.s. velocity profiles in the cylinder wake at $Re = 144$ as a function of downstream distance x/l_F and lateral distance y/d. The cylinder vibrated at $0{\cdot}12d$ at the Strouhal frequency f_s.

sweeping through a cycle of the vortex street from $\xi = 0$ to $\xi = 1$, for chosen values of K, r_* and h/l, and then computing the total mean and r.m.s. velocities based on both u' and v' components at each value of y.

6. Evaluation of the wake response to cylinder vibrations

6.1. *Velocity fluctuations and mean flow*

Both r.m.s. and mean velocities were measured in and downstream of the formation region. The data obtained under one set of conditions, for cylinder vibrations at $f = f_s$ and an amplitude of 12 % of a diameter, are plotted in figure 4. The downstream distance is scaled by l_F and the development of the velocity fields corresponds to the formation region, stable region and early stages of the unstable region outlined in figure 2. A determination of the vortex-street parameters K, r_* or t, and h/l was made at $x = 2{\cdot}2$ and $2{\cdot}6l_F$, and the positions chosen are listed in table 2.

The computations involved in matching the experimental data with the model in § 5 are time consuming, but they can be readily carried out on a digital computer. At each of the chosen values of y/d, the velocity $q' = (u'^2 + v'^2)^{\frac{1}{2}}$ was determined for chosen values of r_* and h/l over 100 steps in the interval $0 \leqslant \xi \leqslant 1$, and

Frequency ratio f/f_s	Amplitude ratio a/d	Wake parameter St^*	Downstream position x/d	x/l_F
1·0	0·12	0·199	6·0	2·3
			6·8	2·6
0·9	0·30	0·208	5·0	2·2
			5·9	2·6
1·0	0·30	0·231	4·4	2·2
			5·2	2·6
1·1	0·30	0·254	3·9	2·2
			4·6	2·6
1·0	0·48	0·263	3·7	2·2
			4·4	2·6

TABLE 2. Locations for the evaluation of vortex-street parameters in the wakes of vibrating cylinders. Reynolds number = 144

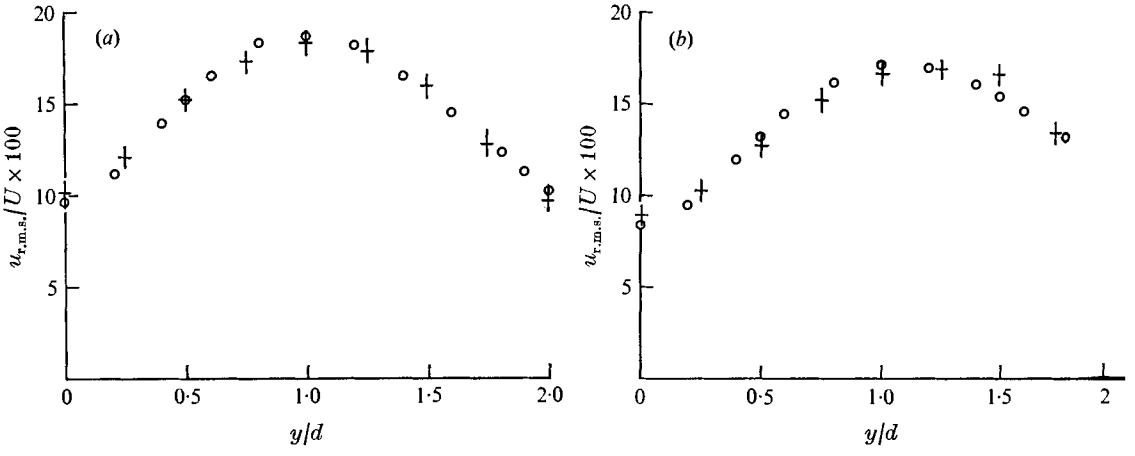

FIGURE 5. Measured and computed r.m.s. velocity profiles in the stable region of the vibrating cylinder wake, at $Re = 144$. (*a*) $f = f_s$, $a = 0{\cdot}3d$, $x = 2{\cdot}2l_F$, $St^* = 0{\cdot}231$. (*b*) $f = 0{\cdot}9f_s$, $a = 0{\cdot}3d$, $x = 2{\cdot}6l_F$, $St^* = 0{\cdot}208$. +, experimental data; ○, computed velocity profiles.

the local mean and r.m.s. velocity computed. An initial guess at K was necessary, but the solution quickly converged and two successive average values of K at all the points were obtained to within an arbitrary $\delta K/K_{\text{av}}$, say 10^{-3}. Thus, a particular triplet of the parameters K, r_* and h/l resulted in a certain error E as given by (4), and the solution was defined as the set of parameters that yielded the minimum error.

Some examples are given in figures 5 and 6 to indicate the agreement between the measured velocity profiles and those generated on the computer. There are only a few determinations of the vortex wake parameters available in the literature for either a laminar or turbulent vortex street and none at all for the case of a vibrating cylinder. Schaefer & Eskinazi (1959) measured the vortex strength at a single point on the wake centre-line $y = 0$, in the stable region of a stationary-cylinder wake at $Re = 62$. Their computed mean and r.m.s. velocity profiles fall

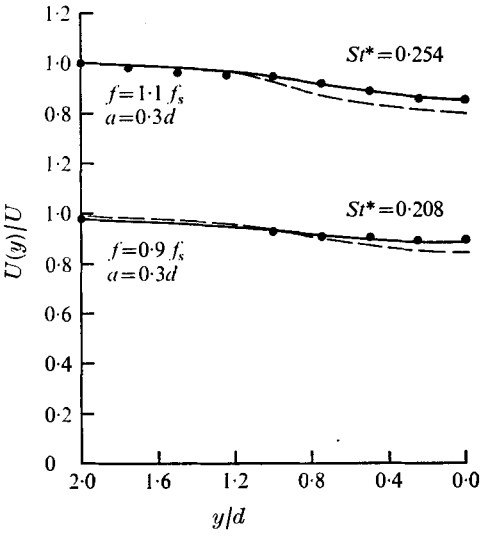

FIGURE 6. Measured and computed mean velocity profiles in the stable region of the vibrating cylinder wake, at $Re = 144$. $x = 2{\cdot}6l_F$. ——, experimental data; – – –, computed profiles.

away considerably from the measured data as the distance from the wake centre-line is increased. Berger (1964) solved for the triplet K, r_* and h/l in the wake of a stationary cylinder by employing three simultaneous equations at arbitrary choices of y/d, and the agreement obtained in this case was somewhat dependent on the choice of the three values of the displacement from the wake centre-line. Bloor & Gerrard (1966), in their measurements of turbulent vortex strength, obtained agreement comparable to the present case only for lateral displacements beyond the maximum of the vortex velocity profile.

6.2. *Strength, age and spacing of the vortices*

The vortex strength should remain constant over a finite length of the wake in order for the assumed velocity distribution to be an optimal approximation for the actual vortex street. The results summarized in table 3 satisfy this criterion to within an acceptable degree, for the downstream positions $x = 2{\cdot}2$ and $2{\cdot}6l_F$. The vortex strength obtained at displacements between 1·0 and $2{\cdot}0l_F$ was not constant, but this is not surprising since the measurements of the velocity field and the wake configuration in figures 2 and 4 show that the street development is still continuing in that region.

The spacing ratio of the vortices decreases as the amplitude of vibration increases, and this is in accord with the photographs described in the next section. All of the results for the spacing ratio h/l from the computer matching are considerably less than the theoretical value of $h/l = 0{\cdot}281$ obtained by von Kármán in his original analysis. The spacing ratio behind the vibrating cylinder decreases from 0·156 to 0·112 as the amplitude of vibration increases from 12 to 48 % of a diameter and, since the longitudinal spacing is independent of the cylinder amplitude, this change is a reflexion of adjustments only in the lateral spacing of

Downstream displacement x/l_F	Shedding parameter St^*	Longitudinal spacing l/d	Formation length l_F/d_F	Vortex core radius r_*/l	Spacing ratio $h/2l$	Vortex strength $K/\pi Ud$
—	0·178	5·4	2·6	0·178	—	0·81†
2·3	0·199	5·4	2·1	0·184	0·078	1·12
2·6	—	—	—	0·187	0·078	1·10
2·2	0·208	5·9	1·8	0·193	0·059	1·28
2·6	—	—	—	0·195	0·063	1·26
2·2	0·231	5·4	1·6	0·192	0·064	1·24
2·6	—	—	—	0·194	0·067	1·22
2·2	0·254	4·9	1·4	0·208	0·067	1·34
2·6	—	—	—	0·210	0·073	1·32
2·2	0·263	5·4	1·2	0·204	0·052	1·36
2·6	—	—	—	0·205	0·056	1·34

† Estimated from the results for the high speed mode of Berger (1964) at $Re = 150$.

TABLE 3. Strength and spacing of the vortices. Reynolds number = 144

the vortices. It is interesting to note that the amplitude and frequency of vibration act on the spacing ratio in different ways. The spacing ratio increases with frequency at fixed amplitude, and this behaviour appears to be principally caused by the inverse dependence of frequency and longitudinal spacing in the regime of synchronization.

The age t of the Hamel–Oseen vortices is also a function of both the amplitude and frequency of vibration, and the results obtained at $x = 2{\cdot}6l_F$ are plotted in figure 7. The apparent age of the vortices increases with increasing amplitude of vibration, but decreases as the vibration frequency is increased at fixed amplitude. The growth rate of the cores

$$m = \frac{\Delta(4\nu t/d^2)}{\Delta(x/d)} = 4\frac{U}{U_\phi}\frac{1}{Re} \tag{5}$$

can be estimated from the speed $U_\phi = fl$ of the vortex centres. This growth rate is linear in the stable region, and therefore

$$\frac{4\nu t}{d^2} = \frac{4\nu t}{d^2}\bigg|_{x=0} + m\frac{x}{d}. \tag{6}$$

As an example, for $a = 0{\cdot}3d$ and $f = f_s$, $m = 0{\cdot}0289$ and $[4\nu t/d^2]_{x=0} = 0{\cdot}73$. This implies that the vortices have a finite age at the cylinder position $x = 0$, and that the apparent origin of the viscous vortices, or the position corresponding to the initial value $t = 0$, lies ahead of the cylinder. For the conditions just mentioned, the origin $x|_{t=0}$ lies at $x = -25d$. The ages $[4\nu t/d^2]_{x=0}$ and the apparent origins for the viscous vortices are listed in table 4, and show that the rate of vortex-core growth and the diffusion of vorticity in the wake are both dependent on the amplitude and frequency of vibration. A value of $x|_{t=0} = -12$ was obtained by Berger (1964) in his study of the stationary-cylinder wake at $Re \approx 150$.

Not only are the spacing ratio, core radius and the vortex age dependent on the vibrations, but also the vortex strength is strongly influenced by the motion of

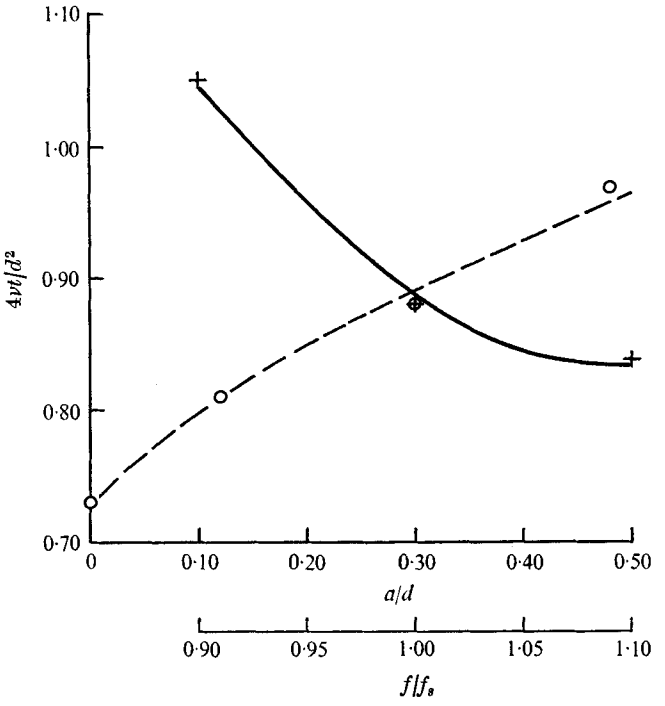

FIGURE 7. The viscous age of the vortices, at $x = 2{\cdot}6l_F$ in the wake of a vibrating cylinder, as a function of the amplitude and frequency of the vibrations. $Re = 144$. – – –, constant frequency, $f = f_s$; ——, constant amplitude, $a = 0{\cdot}3d$.

St^*	$[4\nu t/d^2]_{x=0}$	$[x/d]_{t=0}$
0·178	0·49	−17
0·199	0·61	−21
0·208	0·88	−30
0·231	0·73	−25
0·254	0·71	−24
0·263	0·84	−29

TABLE 4. Viscous age and theoretical origin of Hamel–Oseen vortices. Reynolds number = 144

the cylinder. The final results obtained in the present study are listed in table 3. There is increased vortex strength for all synchronized flow conditions, with greater values of the wake parameter St^* corresponding in general to increased strength of the wake vortices. The vortex strength was increased by as much as 65 % from the stationary-cylinder value for conditions reached in the present experiments.

6.3. *Vortex strength and formation length*

The circulation K is plotted in figure 8 as a function of the ratio l_F/d_F. There is approximately an inverse relationship between the vortex strength and the downstream distance at which the vortices are fully formed, there being an increase in the vortex strength to correspond with a decrease in the formation-region length.

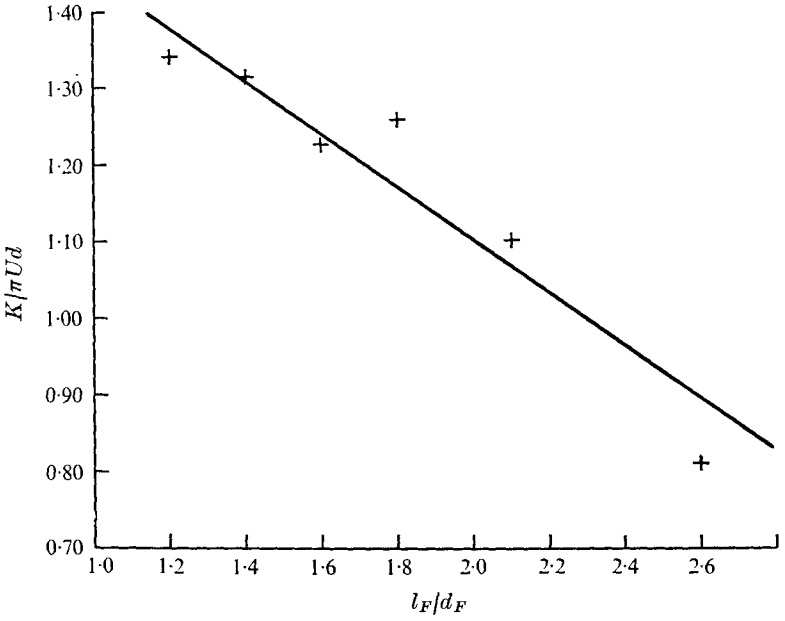

FIGURE 8. The measured relation between the initial circulation K of the vortices and the formation length l_F in the wake of a vibrating cylinder. The wake width at formation is denoted by d_F [see (1)]. $Re = 144$.

All of the measurements made under conditions of synchronization between the vortex and vibration frequencies result in higher vortex strengths and decreased formation lengths relative to those measurements made in the wake of a stationary body.

The changes in the vortex strength and the formation-region length are in accord with the changes that take place in the fluid forces under conditions of both forced and flow-induced synchronization. Protos, Goldschmidt & Toebes (1968), Bishop & Hassan (1964) and Toebes & Ramamurthy (1967) have measured the increased lift that accompanies forced body oscillations. Bishop & Hassan found that the lift coefficient of a cylinder vibrating at $a/d = 0{\cdot}5$ was double the stationary-cylinder value for $f/f_s = 0{\cdot}95$ and $Re = 6000$. Toebes (1969) has measured the decreased base pressure that accompanies forced synchronization and Griffin, Skop & Koopmann (1973) have reported measurements of the increased steady drag force that accompanies the flow-induced oscillations of a circular cylinder at Reynolds numbers between 500 and 900. All conditions of lock-in reported in the latter work resulted in higher drag, with the drag coefficient increasing by as much as 75 %. Tanida, Okajima & Watanabe (1973) have also measured the increased drag that accompanies forced lateral oscillations of a circular cylinder when it is towed through still water. Bearman (1965) has reported the relation between the base pressure coefficient and formation-region length when splitter plates were used to alter the flow in the wake of a blunt-based aerofoil, and here again a nearly inverse relation between the base pressure coefficient and formation length was found.

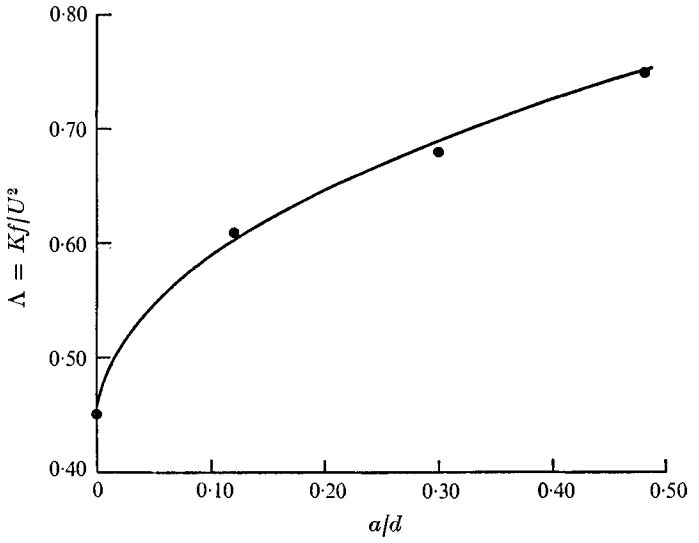

FIGURE 9. The rate Λ of vorticity generation as a function of the cylinder amplitude of vibration at the Strouhal frequency f_s. $Re = 144$.

6.4. *Vorticity generation in the wake*

Once the vortex strength or circulation has been obtained, it is possible also to obtain a measure of the response of the wake to the vibrations in terms of Λ, the rate of vorticity generation per unit time. This can be written in non-dimensional form as

$$\Lambda = \frac{Kf}{U^2} = \pi St\left(\frac{f}{f_s}\right)\left(\frac{K}{\pi Ud}\right) \tag{7}$$

in terms of the initial circulation K of the fully developed street, the vibration (and vortex shedding) frequency f and the free-stream speed U. The magnitude of Λ obtained from the fully developed street is less than the vorticity shed at the cylinder, so that the fully developed value takes account of the mixing of vorticities of opposite sign in the formation region and the ensuing development of the vortices in the early part of the stable region shown in figure 2.

The response of the wake, in terms of Λ, to the amplitude of the oscillations at the Strouhal frequency f_s is plotted in figure 9. The rate of vorticity generation increases by 50 % at an amplitude of $0{\cdot}30d$ and by 70 % at $0{\cdot}48d$ from the result obtained in the wake of the stationary cylinder. In figure 10 the variation of Λ with frequency within the synchronized regime is plotted, and again there is a response of the wake to the vibrations. When the vibration frequency is 110 % of the Strouhal frequency at an amplitude of $0{\cdot}30d$, Λ is increased by 80 % from the result obtained in the wake of a stationary cylinder.

7. Flow visualization of vortex formation and spacing

All of the flow-visualization experiments described in this section were performed at a Reynolds number of 190. An appropriate flow speed corresponding to this particular Reynolds number represented a set of optimal conditions for

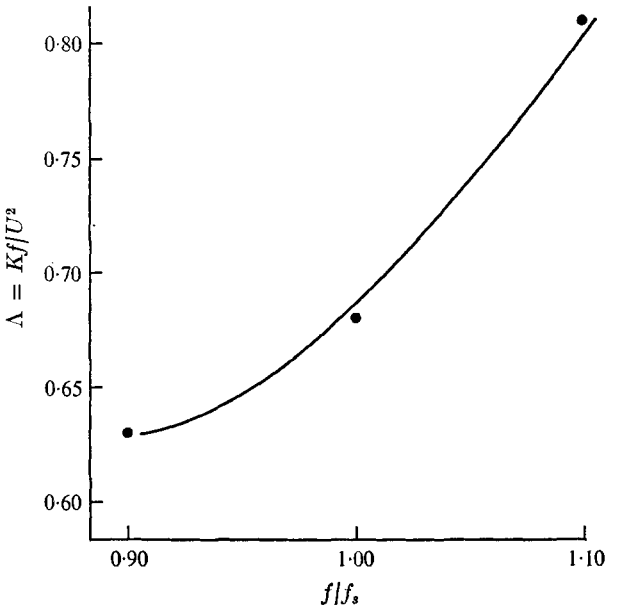

FIGURE 10. The rate Λ of vorticity generation as a function of the frequency ratio f/f_s, for synchronized cylinder vibrations at $Re = 144$ with the amplitude of oscillation held constant at $a = 0{\cdot}30d$.

(Peak-to-peak amplitude/diameter) × 100				
f/f_s = 0·85	0·90	1·00	1·05	1·10
—	—	0	—	—
—	—	10	—	—
—	20	20	—	20
30	30	30	30	30
50	50	50	50	50
—	—	—	—	60
80	80	80	80	—
100	100	100	—	—
—	—	120	—	—
—	—	130	—	—
—	—	150	—	—

TABLE 5. Vibration amplitude and frequency for the flow-visualization experiments. Reynolds number = 190; Strouhal shedding frequency = 36·5 Hz

the simultaneous operation of one of our aerosol generators and the wind tunnel. By an appropriate choice of cylinder diameter (4 mm), the experiments were performed in the Reynolds number range (Re = 125–350) where lateral vibrations of the cylinder synchronize with the vortex shedding, stabilize the wake and delay the initiation of turbulence, which usually occurs in a vortex street at Reynolds numbers above 125. Conditions of vibration amplitude and frequency at which photographs of the wake were taken are listed in table 5. The threshold amplitude at which lock-in was initiated varied with frequency. When the

vibration frequency was $0{\cdot}85f_s$ the threshold occurred at $a = 0{\cdot}25$–$0{\cdot}30d$ whereas the threshold decreased to $a = 0{\cdot}20d$ for $f = 0{\cdot}9f_s$. At the Strouhal frequency, lock-in was observed at an amplitude $a = 0{\cdot}10d$ while at $f = 1{\cdot}10f_s$ the threshold amplitude again increased to $a = 0{\cdot}15$–$0{\cdot}20d$. These observations are in good agreement with results originally published by Koopmann (1967*a*).

7.1. *The effects of vibration amplitude and frequency on street spacing*

In the preceding section of this work, matching a mathematical model for the vortex street with measured velocity profiles has indicated that the lateral vortex spacing in the stable region of the wake decreases as the amplitude of vibration increases. A series of photographs taken at increasing vibration amplitudes is shown in figures 11(*a*)–(*e*) (plate 1). The longitudinal spacing of the vortices remains fixed at the same value as that for a stationary cylinder for these vibrations at the Strouhal frequency. There is, however, some appearance of decreasing lateral spacing and greater regularity in the downstream wake of the vibrating cylinder, even at amplitudes of 10 and 20 % of a diameter. The formation length also decreases from about $2{\cdot}5$ to $1{\cdot}5d$ as the amplitude increases from zero to half a diameter in this series of photographs.

Although there is some indication at the lower vibration amplitudes that the viscous cores of the vortices begin to interact downstream, this behaviour is readily apparent in the photographs taken at vibration amplitudes of $0{\cdot}5$ and $0{\cdot}8d$. At these large amplitudes the street approaches a single line of vortices of alternating sign and the vortex cores begin to interact much closer to the cylinder. Measurements made with hot wires and reported earlier in II and III have shown that this unstable behaviour is dependent on both the amplitude and frequency of the oscillations. The unstable region is characterized by vortex distortion and elongation as seen in figures 11(*d*) and (*e*), and by the reappearance of large deficits of the mean velocity in that region where the vortex cores begin to interact. Increased vortex strength and vorticity generation accompany these changes in spacing in the stable region of the vortex wake as the amplitude of motion is increased.

Not only do changes in cylinder amplitude affect the wake structure, but also the vibration frequency controls the development of the vortex street behind the cylinder. The rate of vorticity generation, the viscous vortex age and the street spacing ratio all are dependent on the frequency. Several photographs are shown in figures 12(*a*)–(*e*) (plate 2), for experiments in which the amplitude of oscillation was held constant at $0{\cdot}30d$ while the frequency changed from 85 to 110 % of the Strouhal value.

Since all of the photographs were taken at the same settings and relative positions, it is possible to make comparative estimates of the longitudinal vortex spacing from the figures. As the frequency changes from $0{\cdot}85$ to $1{\cdot}10f_s$, there is a decrease of about 35 % in the longitudinal spacing. This agrees reasonably well with the hot-wire measurements made at $Re = 144$, from which the longitudinal spacing was found to be inversely proportional to the frequency. The length of the formation region of the vortices decreases from $2{\cdot}2$ to $1{\cdot}5d$ for the conditions shown in figure 12, and also varies inversely with the vibration frequency.

As the frequency is increased within the lock-in regime, the unstable region of the wake moves upstream, towards the cylinder. This becomes increasingly apparent in figures 12(*d*) and (*e*), where the flow along the centre-line of the wake becomes irregular and breaks down to turbulence as the oscillation frequency approaches the upper limit of the locking-in. The elongation and distortion of the vortex cores are again visible, especially in figures 12(*d*) and (*e*), and are accompanied by the reappearance of a large deficit in the mean flow in the unstable region.

The lateral vortex spacing in the stable region appears to undergo little change with vibration frequency, as the principal length scales that determine the wake pattern are the formation-region length l_F, the longitudinal vortex spacing l and the length l_s of the stable region. The stable-region length is governed by the rate of core growth after a vortex is fully formed and shed from the base region of the cylinder, and the results in II have indicated that the ratio l_s/l_F is a function of only the Reynolds number when the wake and vibration frequencies are locked together.

7.2. *Vortex streets at large amplitudes of vibration*

The vortex streets just discussed were generated when the cylinder was vibrating at amplitudes of less than a diameter. It is interesting to observe some of the effects of large amplitude vibrations, i.e. amplitudes near or greater than a full diameter of the cylinder. Three particular conditions have been chosen, at vibration frequencies of 85, 90 and 100 % of the Strouhal value, at a Reynolds number of 190.

Three photographs taken at $f = 0{\cdot}85f_s$ are shown in figures 13(*a*)–(*c*) (plate 3). The cylinder was vibrating at an amplitude of half a diameter when figure 13(*a*) was taken, and the street is very nearly a single line of vortices of alternating sign. As the cylinder amplitude was increased further, to 80 % of a diameter, as shown in figure 13(*b*), a most peculiar form of vortex street began to emerge. The vortex of counterclockwise rotation shed from the lower portion of the cylinder shows evidence of breaking up into two vortices of like sign. When the amplitude of vibration is increased to a full diameter, there are two fully developed counterclockwise vortices being formed during each cycle of the cylinder motion while only a single clockwise vortex is shed in the usual manner.

Further evidence of this behaviour is shown in figures 14(*a*)–(*c*) (plate 4). These photographs were taken with the cylinder vibrating at the Strouhal frequency and at amplitudes in excess of a diameter. The effects of increasing the cylinder amplitude of motion at the Strouhal frequency have so far been discussed just for amplitudes up to 80 % of a diameter. When the amplitude was increased to 120 % of the diameter, the resulting wake pattern was as in figure 14(*a*). There is evidence of intense interaction between the vortices downstream, together with distortion of both the cores and the instantaneous filament lines that divide the fluid that has passed on either side of the cylinder. As the amplitude was increased still further, as shown in figure 14(*b*), there was further distortion of the cores and filament lines downstream. This region of interaction was again preceded by a vortex street with very small lateral spacing. The wake pattern in figure 13(*c*), obtained with the cylinder vibrating at 150 % of a diameter, shows once more the

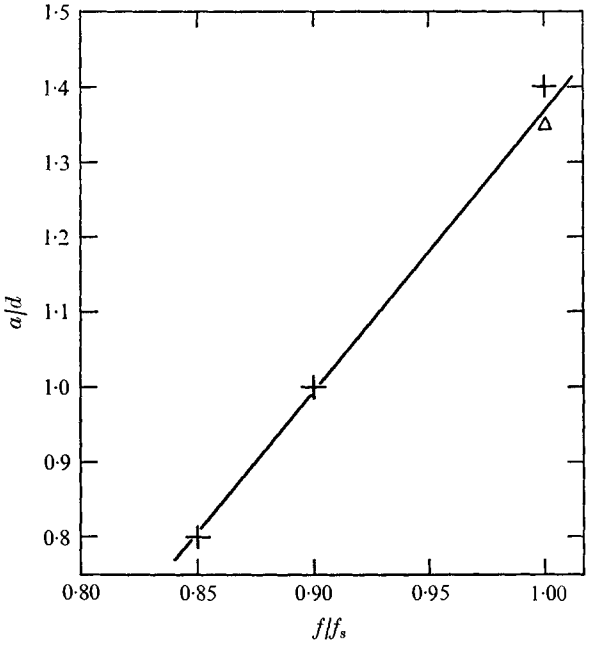

FIGURE 15. The critical amplitude a/d of cylinder vibration, at several frequencies of oscillation. +, Reynolds number = 190; △, Reynolds number = 144.

initiation of secondary vortices at the cylinder and their development with downstream distance.

Such behaviour was observed under other conditions listed in table 5 but is not discussed in detail here. When the cylinder was vibrated at 90 % of the Strouhal frequency, the usual decrease in lateral spacing was observed as the amplitude of motion was increased, and the incipient stages of the secondary vortex formation were observed at an amplitude of one diameter. The amplitude of vibration at which the vortex street appears to undergo a transition with secondary vortex formation is plotted in figure 15. Honji & Taneda (1968*a*) mentioned the appearance of this transition although they did not discuss it in detail.

The breakup of a vortex pattern of vanishing lateral spacing, similar to that of figure 14(*b*), has recently been generated in the computer experiments of Christiansen & Zabusky (1973). The fission or breakup of a finite street of collinear vortices was generated in the computer experiments only for the limiting case $Re \to \infty$ (Christiansen 1974, private communication), while such behaviour was observed in the present experiments at $Re = 190$.

A possible explanation of this phenomenon may be found in the observed dependence of lateral street spacing on the amplitude of vibration. The lateral spacing becomes smaller as the amplitude of vibration increases, and it appears that the initiation of the secondary vortex formation is related to the limit $h/l \to 0$. Further support for this explanation appears in figure 16, where the values of spacing ratio from table 3 are plotted as a function of cylinder amplitude. Extrapolating these results to the limiting case of zero spacing yields a predicted critical vibration amplitude of 130–140 % of a diameter. The predicted onset of

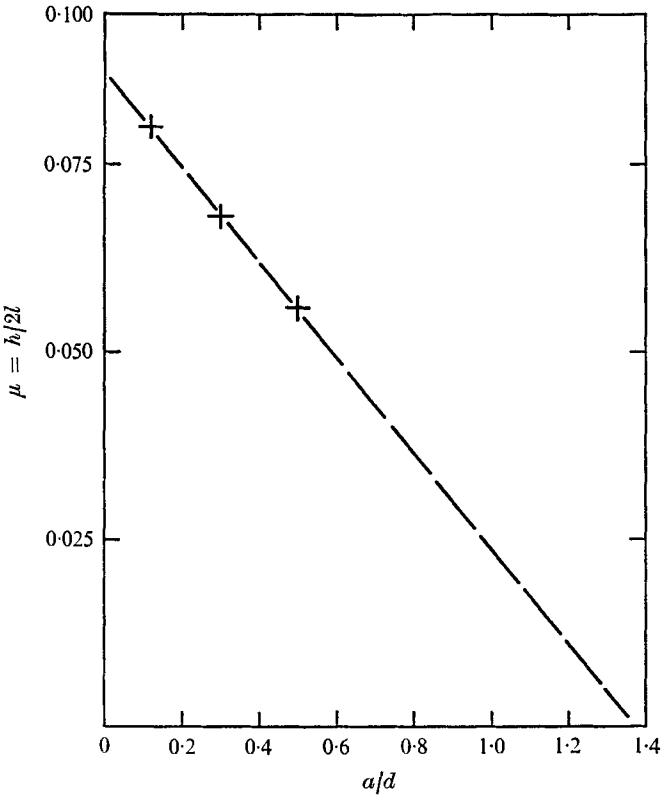

FIGURE 16. The effects of cylinder vibration amplitude on the vortex-street spacing ratio $\mu = h/2l$ in the stable region of the vortex street. The cylinder was vibrated at the Strouhal frequency with a Reynolds number of 144.

the secondary vortex formation compares well with the measured results in figure 15 for similar conditions at $Re = 190$.

The limit $h/l = 0$ is related to the transition from a drag- to a thrust-type street where the induced street velocities and fluid forces on the cylinder in the direction of flow change sign. There appears to be a transition to the asymmetric configurations in figures 13(*c*) and 14(*c*) in order to preclude the development of a thrust-type street of vortices as the cylinder amplitude is increased beyond a critical value corresponding to zero lateral spacing.

7.3. *Flow visualization of the vortex formation process*

Gerrard (1966) has proposed a physical model for the vortex shedding from a bluff body, and the vibrating-cylinder wake at Reynolds numbers between 150 and 300 provides ideal conditions for further study of Gerrard's model by examining the flow in the formation region. The vortex shedding is uniform along the cylinder axis and the wake is two-dimensional in the formation and stable regions. A sequence of photographs, taken over one cycle of cylinder motion, is presented in figures 17(*a*)–(*l*) (plates 5 and 6). The cylinder was vibrating at 85 % of the Strouhal frequency and at an amplitude of 0·50*d*.

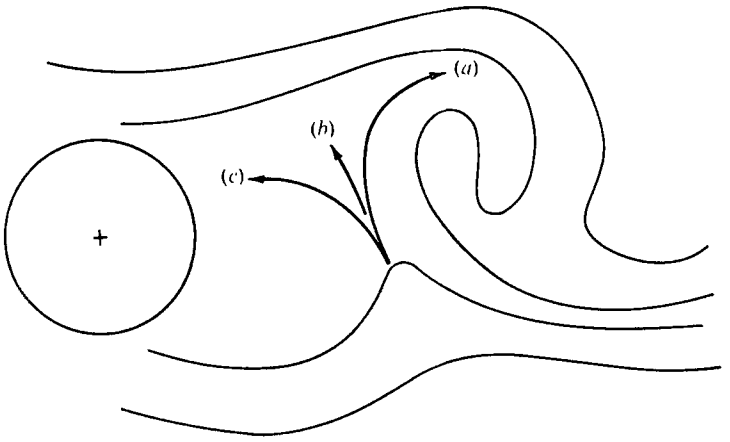

FIGURE 18. A sketch of the instantaneous filament lines in the formation region behind a cylinder (after Gerrard 1966). The arrows show (*a*), (*b*) entrainment and (*c*) reverse flow.

A photograph was taken every 30° during a cycle of the motion and the cylinder is at the uppermost position of its cycle in figure 17(*a*). Under these conditions the formation region, as measured by the criteria mentioned in § 5, extends about 1·9–2·0*d* downstream.

Basically, Gerrard has postulated that a growing vortex is fed by circulation from the separated shear layers until it is strong enough to begin rolling up and drawing the opposing shear layer across the wake. The approach of vorticity of opposite sign then cuts off further circulation to the growing vortex, which is shed and moves downstream. This process continues at a particular frequency to form a vortex street behind a bluff body. A sketch is given in figure 18 to illustrate the basic process suggested by Gerrard in his paper. The filament lines are shown at the instant that fluid from outside the wake is about to be drawn across the formation region, and the arrows indicate the motion of this fluid at later times. Part of the fluid is entrained by the growing vortex and part by the separating shear layer. The remainder (*c*) of the fluid is transferred to the interior of the formation region adjacent to the body base. The photograph in figure 17(*c*) is virtually identical to Gerrard's original sketch.

A growing vortex behind the vibrating cylinder rolls up more quickly, draws the opposing shear layer across the wake and is shed at a smaller downstream distance as the amplitude of vibration is increased. When the frequency is varied about the Strouhal value, the formation region is either expanded or contracted, depending upon whether the frequency ratio is less or greater than unity. These latter effects are in accord with the splitter-plate experiments of Gerrard (1966) and Bearman (1965), where the wake frequency was dependent on the expansion or contraction of the formation region with wake splitter plates. Conversely, the scale of the formation region responds to changes in the frequency of the lateral vibrations in accordance with Gerrard's model.

Several features of the wake behind the vibrating cylinder serve to elucidate Gerrard's description of the vortex formation process. The photographs in figure 17 clearly indicate the regions of fluid that have passed on either side of

the cylinder, and the formation region can be easily identified since it is virtually devoid of aerosol. During the portion of the motion depicted in the first four frames, a vortex is being formed as the shear layer separates from the upper extremity of the cylinder. The cylinder begins its downward motion and the entrainment of fluid from the interior of the formation region (see figure 18) is indicated by the dark area in the growing vortex. As the cylinder reaches the position shown in figure 17 (*d*), the upper vortex is fully formed and another of opposite sign has begun to form and to draw the fluid passing above the cylinder across the wake. The motion of the shear layers and separation zones is evident throughout the sequence also; as the cylinder moves downward, the shear layers appear to move counterclockwise, while as the cylinder begins its upward motion, cf. figure 17 (*g*), the shear layers appear to move clockwise throughout much of the remainder of the sequence. Mei & Currie (1969) have measured with a hot wire the motions of the separation zone and the shear layers as a cylinder undergoes vortex-excited lateral vibrations, and have found both the mean and fluctuating positions of the separation zone to be responsive to changes in the amplitude and frequency of vibration.

The wake patterns behind the vibrating cylinder support in detail Gerrard's model for the transfer of circulation and vortex formation in the base region of a bluff body. The entrainment of fluid from inside the formation region by the growing vortex, and the drawing of fluid from outside the wake across the formation region have been observed in detail here. Fluid which has passed either side of the cylinder has been clearly delineated at each instant in a cycle of the cylinder's travel, and the instantaneous wake patterns in figure 17 also reveal the mixing processes that take place in the vortex street after formation. Fluid which has passed on one side of the cylinder is drawn across the wake centre-line downstream of formation, and this mixing of fluid containing vorticity of opposite sign contributes to the rapid reduction in velocity fluctuations during the development of the street. The vortex formation and mass-transfer processes in the wake of a stationary cylinder at low Reynolds numbers ($Re \sim 100$) have been observed by Zdravkovich (1969).

8. Summary and conclusions

The aim of this programme was to measure the changes in vortex strength and spacing that accompany different conditions of oscillation of a circular cylinder under conditions of synchronization between the vortex shedding and vibration frequencies, and thereby to obtain some further insight into the interaction between a vortex-street wake and a vibrating bluff body.

A mathematical model for the vortex street was matched with measured r.m.s. and mean velocity profiles at two downstream locations in the stable region of the street at a Reynolds number of 144. The strength, viscous vortex age and spacing ratio of the street were obtained by satisfying a minimum-error criterion. The stable vortex street contains a regime of essentially constant vortex strength where the lateral spacing changes only slightly.

An inverse relation was found between the initial circulation (or strength)

of the vortices and the formation-region length at amplitudes of vibration up to at least 50 % of a diameter, where the initial circulation was increased by 65 % from its value in the stationary-cylinder wake. A corresponding inverse relation between the base pressure or drag and the formation-region length has been obtained by others.

The rate Λ of vorticity generation in the wake is a function of both the amplitude and frequency of vibration. An increase in Λ of 80 % from the stationary-cylinder wake value was obtained with the cylinder vibrating at $0{\cdot}30d$ and 110 % of the Strouhal frequency.

The lateral spacing of the vortex street decreases with increasing amplitude of cylinder vibration, but the longitudinal spacing remains constant so long as the frequency does not change. At a Reynolds number of 190, the length of the formation region of the vortex street decreased from $2{\cdot}5$ to $1{\cdot}5d$ in length as the vibration amplitude increased from zero to half a diameter.

The longitudinal vortex spacing varies inversely with vibration frequency in the regime where the body and wake frequencies are synchronized. When the vibration frequency was increased from 85 to 110 % of the Strouhal frequency, at an amplitude of 30 % of a diameter, the formation-region length decreased from $2{\cdot}2$ to $1{\cdot}5d$ and the longitudinal vortex spacing decreased by 35 %. The lateral spacing changed little with changes in frequency.

Vortex-street formation as the cylinder undergoes large amplitude lateral vibrations has been observed. As the amplitude is increased at different frequencies the street approaches a single line of vortices of alternating sign. Secondary vortex formation at these large amplitudes near a full diameter is associated with the limit of the street spacing ratio $h/l = 0$. As this limit is approached there is an alteration in the street configuration to preclude the transition from a drag- to a thrust-type street.

Observation of the wake behind a vibrating cylinder serves to elucidate the mechanism of the vortex formation process. The entrainment, by a growing vortex, of fluid from inside the formation region and the drawing across the formation region of fluid from outside the wake have been observed at small intervals over a cycle of the cylinder motion.

The writers wish to acknowledge the support of the Naval Research Laboratory (NRL) for the research programme that resulted in this paper. Special thanks also go to the NRL Photography staff for many helpful suggestions. These results were presented at the 7th U.S. National Congress of Applied Mechanics.

REFERENCES

Bearman, P. W. 1965 *J. Fluid Mech.* **21**, 241–255.
Berger, E. W. 1964 *Z. Flugwiss.* **12**, 41–59.
Berger, E. W. & Wille, R. 1972 *Ann. Rev. Fluid Mech.* **4**, 313–340.
Bishop, R. E. D. & Hassan, A. Y. 1964 *Proc. Roy. Soc.* A **277**, 51–75.
Bloor, M. S. & Gerrard, J. H. 1966 *Proc. Roy. Soc.* A **294**, 319–342.
Chaplin, J. R. 1972 *Trans. A.S.M.E., J. Engng Indust.* **94**, 169–621.
Christiansen, J. P. & Zabusky, N. 1973 *J. Fluid Mech.* **61**, 219–243.

GERRARD, J. H. 1966 *J. Fluid Mech.* **25**, 401–413.

GRIFFIN, O. M. 1971 *Trans. A.S.M.E., J. Appl. Mech.* **38**, 729–738.

GRIFFIN, O. M. 1973 *Trans. A.S.M.E., J. Fluids Engng*, **95**, 579–581.

GRIFFIN, O. M., RAMBERG, S. E., VOTAW, C. W. & KELLEHER, M. D. 1973 *Proc. Int. Cong. on Instrumentation in Aerospace Simulation Facilities* (*I.E.E.E.*), pp. 133–139.

GRIFFIN, O. M., SKOP, R. A. & KOOPMANN, G. H. 1973 *J. Sound Vib.* **31**, 235–248.

GRIFFIN, O. M. & VOTAW, C. W. 1972 *J. Fluid Mech.* **55**, 31–48.

HONJI, H. & TANEDA, S. 1968*a* *Rep. Res. Inst. Appl. Mech.* **16**, 211–222.

HONJI, H. & TANEDA, S. 1968*b* *Bull. Res. Inst. Appl. Mech.* **30**, 4–11 (in Japanese).

KING, R., PROSSER, M. J. & JOHNS, D. J. 1973 *J. Sound Vib.* **29**, 169–188.

KOOPMANN, G. H. 1967*a* *J. Fluid Mech.* **28**, 501–512.

KOOPMANN, G. H. 1967*b* M.S. thesis, Catholic University, Washington.

MAIR, W. A. & MAULL, D. J. 1971 *J. Fluid Mech.* **45**, 209–224.

MEI, V. C. & CURRIE, I. G. 1969 *Phys. Fluids*, **12**, 2248–2254.

PARKINSON, G. V. 1972 Mathematical models for flow-induced oscillations of bluff bodies. *IUTAM–IAHR Symp. on Flow-Induced Structural Vibrations, Invited Paper.*

PROTOS, A., GOLDSCHMIDT, V. & TOEBES, G. 1968 *Trans. A.S.M.E., J. Basic Engng*, **90**, 178–386.

ROSHKO, A. 1954 *N.A.C.A. Tech. Note*, no. 3169.

SCHAEFER, J. W. & ESKINAZI, S. 1959 *J. Fluid Mech.* **6**, 241–260.

TANIDA, Y., OKAJIMA, A. & WATANABE, Y. 1973 *J. Fluid Mech.* **61**, 769–784.

TOEBES, G. H. 1969 *Trans. A.S.M.E., J. Basic Engng*, **91**, 493–505.

TOEBES, G. H. & RAMAMURTHY, A. S. 1967 *Proc. A.S.C.E., J. Engng Mech.* **93**, 1–20.

WEIHS, D. 1972 *J. Fluid Mech.* **54**, 679–690.

WOOD, C. J. 1971 *J. Sound Vib.* **14**, 91–102.

WOOD, C. J. & KIRMANI, S. F. A. 1970 *J. Fluid Mech.* **41**, 627–640.

ZDRAVKOVICH, M. M. 1969 *J. Fluid Mech.* **37**, 491–496.

(*a*)

(*b*)

(*c*)

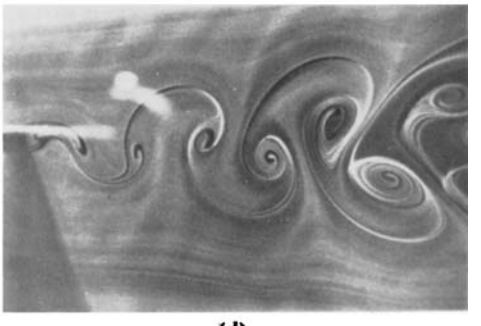

(*d*)

(*e*)

FIGURE 11. The effects on the vortex wake of lateral cylinder vibration at the Strouhal frequency at a Reynolds number of 190. $f = f_s = 36{\cdot}6$ Hz for all figures. (*a*) Stationary cylinder, (*b*) $a = 0{\cdot}10d$, (*c*) $a = 0{\cdot}20d$, (*d*) $a = 0{\cdot}50d$, (*e*) $a = 0{\cdot}80d$.

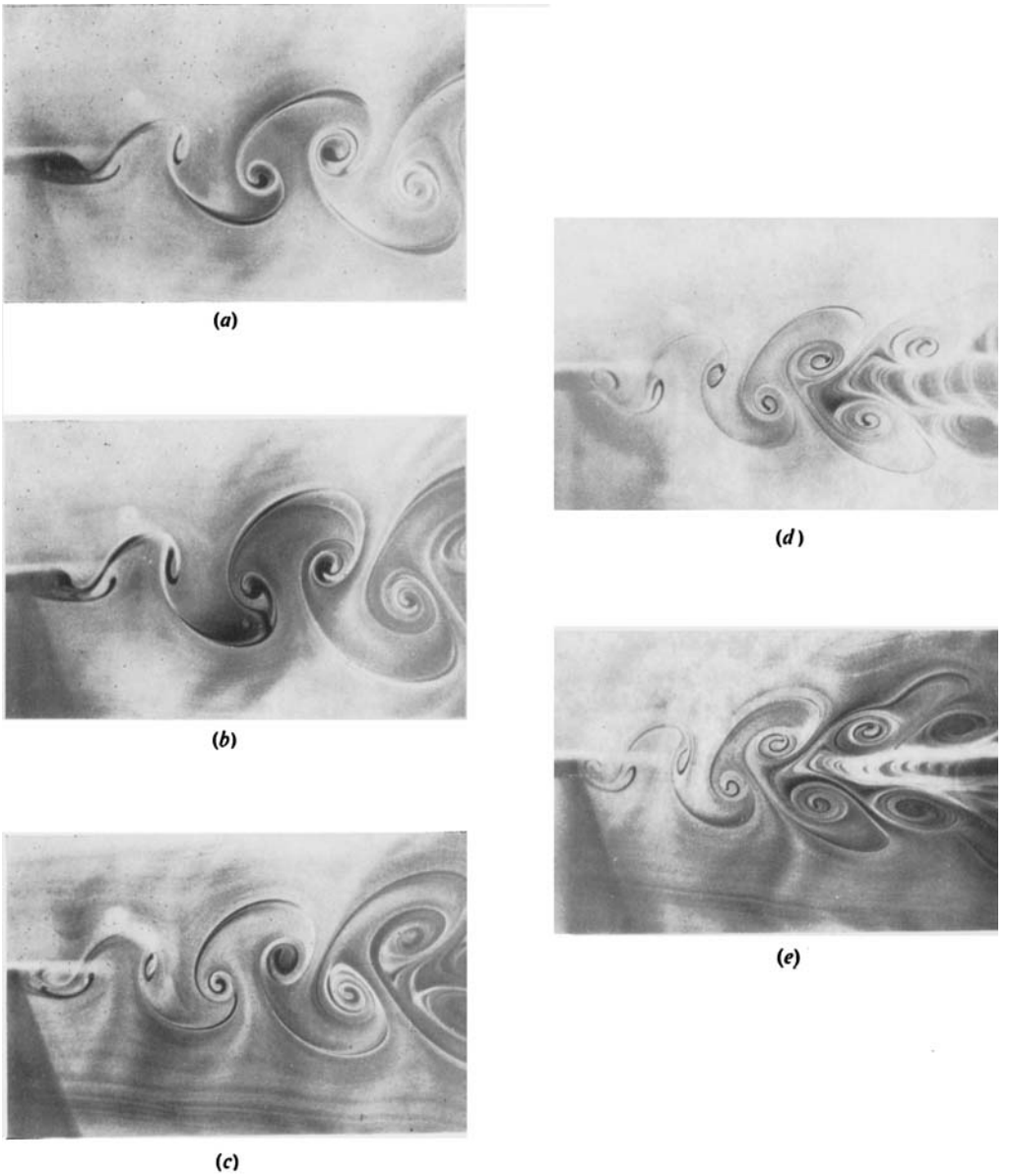

FIGURE 12. The effects on the vortex wake of cylinder vibration frequency at a Reynolds number of 190. The cylinder and wake frequencies were synchronized and the amplitude of vibration was held constant at $0{\cdot}3d$. (*a*) $f = 0{\cdot}85f_s$, (*b*) $f = 0{\cdot}90f_s$, (*c*) $f = f_s = 36{\cdot}6$ Hz, (*d*) $f = 1{\cdot}05f_s$, (*e*) $f = 1{\cdot}10f_s$.

(*a*)

(*b*)

(*c*)

FIGURE 13. Large amplitude lateral motion of a cylinder oscillating synchronized with its vortex wake at a Reynolds number of 190. The vibration frequency was held constant at 85 % of the Strouhal frequency. (*a*) $a = 0{\cdot}5d$, (*b*) $a = 0{\cdot}8d$, (*c*) $a = 1{\cdot}0d$.

(*a*)

(*b*)

(*c*)

FIGURE 14. Large amplitude lateral motion of a cylinder oscillating synchronized with its vortex wake at a Reynolds number of 190. The vibration frequency was equal to the Strouhal frequency. (*a*) $a = 1{\cdot}2d$, (*b*) $a = 1{\cdot}3d$, (*c*) $a = 1{\cdot}5d$.

(*a*)

(*d*)

(*b*)

(*e*)

(*c*)

(*f*)

FIGURES 17 (*a*)–(*f*). For legend see over.

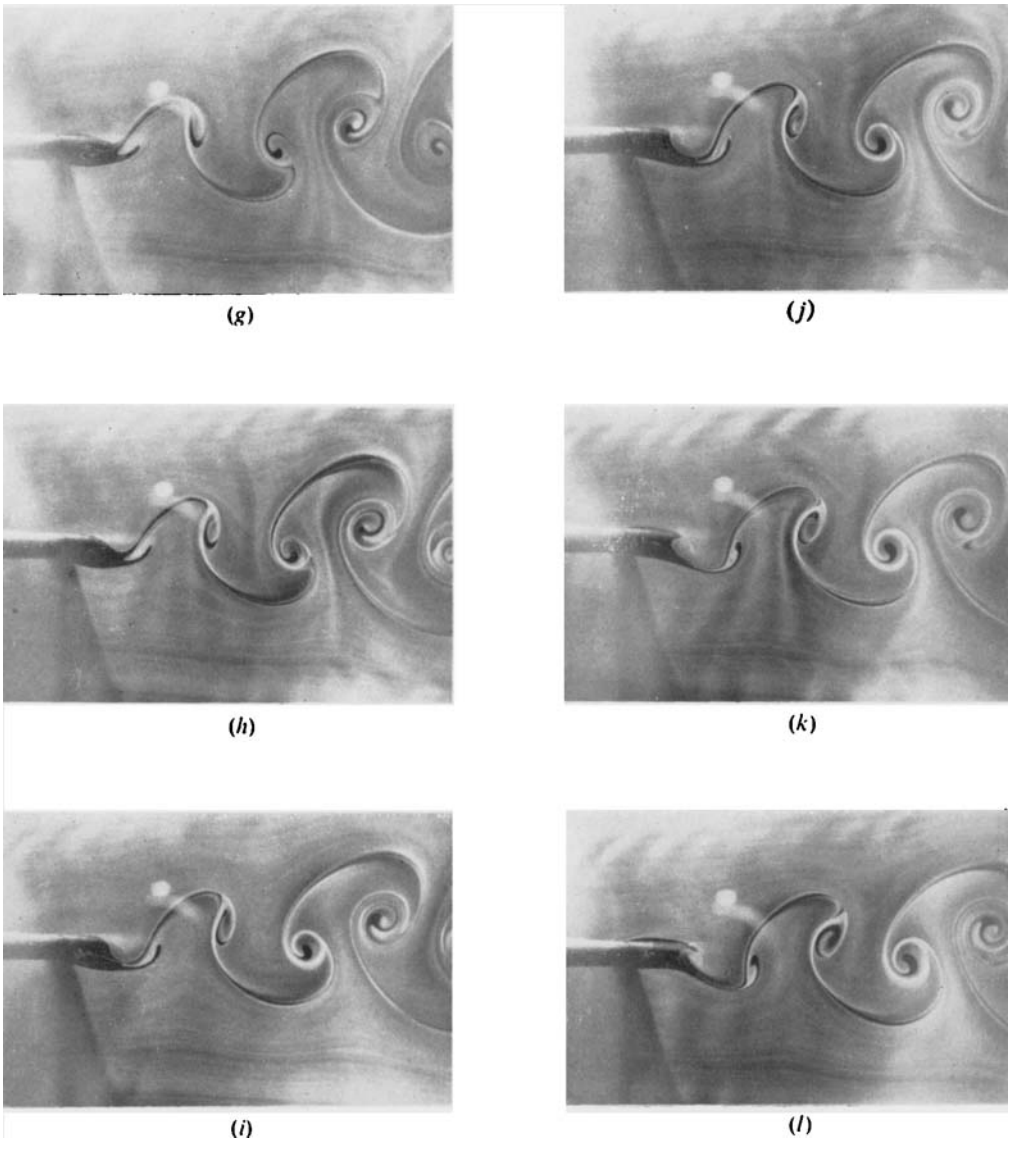

FIGURE 17. Vortex-street formation during a cycle of the motion of a vibrating cylinder. The wake and vibration frequencies were synchronized at 85 % of the Strouhal frequency and a motion amplitude of 0·5d, with a Reynolds number of 190. The cylinder was at its uppermost position in frame (a) and photographs thereafter were taken at increments of 30° in the motion cycle.